ADVANCED FUNCTIONAL MATERIALS
www.afm-journal.de

Materials Views
www.MaterialsViews.com

# Flexible Hybrid Paper Made of Monolayer $Co_3O_4$ Microsphere Arrays on rGO/CNTs and Their Application in Electrochemical Capacitors

*Changzhou Yuan,* Long Yang, Linrui Hou, Jiaoyang Li, Yaxin Sun, Xiaogang Zhang,* Laifa Shen, Xiangjun Lu, Shenglin Xiong,* and Xiong Wen (David) Lou**

**A facile one-step hydrothermal method is developed for large-scale production of well-designed flexible and free-standing $Co_3O_4$/reduced graphene oxide (rGO)/carbon nanotubes (CNTs) hybrid paper as an electrode for electrochemical capacitors. Densely packed unique $Co_3O_4$ monolayer microsphere arrays uniformly cover the surface of the rGO/CNTs film. The alkaline hydrothermal treatment leads to not only the deposition of $Co_3O_4$ microspheres array, but also the reduction of the GO sheets at the same time. The unique hybrid paper is evaluated as an electrode for electrochemical capacitors without any ancillary materials. It is found that the obtained hybrid flexible paper, composed of $Co_3O_4$ microsphere array anchored to the underling conductive rGO/CNTs substrate with robust adhesion, is able to deliver high specific capacitance with excellent electrochemical stability even at high current densities, suggesting its promising application as an efficient electrode material for electrochemical capacitors.**

## 1. Introduction

Electrochemical capacitors (ECs), as a promising energy conversion/storage and power output technology for digital communications and hybrid electronic vehicles, have attracted tremendous interest because of their advantages of higher power delivery and better cycling lifespan over batteries.[1–4] The capacitance of conventional electrical double-layer capacitors (EDLCs) originates from the sole charge separation occurring at the electrode/electrolyte interface. The resultant specific capacitance (SC) is not able to meet the ever-growing need for peak-power assistance in electric vehicles.[1–4] While electrochemical pseudocapacitors (ECPs) using metal hydroxides and/or oxides and conductive polymers exhibit much higher SC and energy density due to their reversible multi-electron redox Faradaic reactions.[5–14] Among these materials, cobalt (II, III) oxide ($Co_3O_4$) has been conceived as a promising electroactive material with great potential to replace the state-of-the-art ruthium dioxide in view of its low cost, high redox activity, large theoretical SC (3560 F $g^{-1}$), great reversibility, and a more environment-friendly nature.[5–11] However, it is still challenging and imperative to develop efficient but simple ways to enhance the utilization of electroactive $Co_3O_4$, particularly at high rates, considering the observed SCs are much lower than its theoretical value.

Up to now, most of $Co_3O_4$-based electrodes for electrochemical evaluation in the literature are commonly binder-enriched electrodes produced by the traditional slurry-coating technology,[6–11] in which a large portion of surface of electroactive $Co_3O_4$ is blocked from the contact with the electrolyte ions to participate in Faradaic reactions for energy storage. Furthermore, the binder involved will greatly decrease the electrical conductivity of the electrode materials, hindering their potential application in high-performance ECs. Therefore, to achieve ideal electrochemical performance, it is important to directly disperse and wire up electroactive $Co_3O_4$ to an underlying conductive substrate. In this regard, novel, free-standing and binder-free electrodes for ECs are highly desirable because such electrodes not only avoid the conventional tedious process of electrode making but also make electroactive $Co_3O_4$ with its large naked surface in direct contact with electrolyte and better electric contact with substrates for efficient energy storage at large current densities.

Recently, flexible films composed of 1D carbon nanotubes (CNTs) and 2D reduced graphene oxide (rGO) have been extensively studied in lithium-ion batteries (LIBs), ECs, and transparent conductors.[15–20] The CNTs in the flexible rGO/CNTs film

Dr. C. Yuan, L. Yang, Dr. L. Hou, J. Li, Dr. Y. Sun
Anhui Key Laboratory of Metal Materials and Processing
School of materials Science and Engineering
Anhui University of technology
Ma`anshan, 243002, P. R. China
E-mail: ayuancz@163.com
Dr. C. Yuan, Prof. X. W. (D.) Lou
School of Chemical and Biomedical Engineering
Nanyang Technological University
70 Nanyang Drive, 637457, Singapore
E-mail: XWLou@ntu.edu.sg
Prof. X. Zhang, Dr. L. Shen, Dr. X. Lu
College of Material Science & Engineering
Nanjing University of Aeronautics and Astronautics
Nanjing, 210016, P. R. China
E-mail: azhangxg@163.com
Prof. S. Xiong
Key Laboratory of Colloid and Interface Chemistry (Shandong University)
Ministry of Education
and School of Chemistry and Chemical Engineering
Shandong University, Jinan 250100, P. R. China
E-mail: chexsl@sdu.edu.cn

DOI: 10.1002/adfm.201102860

not only efficiently increase the basal spacing but also bridge the defects for electron transfer between rGO nanosheets.[16] Thus, the unique rGO/CNTs film, while remaining perfect flexibility, displays even better electrochemical performance and higher electronic conductivity than the single-component rGO film.[16] Therefore, the flexible rGO/CNTs film would be a perfect substrate to deposit $Co_3O_4$ for ECs applications in view of its admirable electronic conductivity and good flexibility.

Here, we report a facile but efficient route to synthesize flexible and free-standing $Co_3O_4$/rGO/CNTs hybrid paper for ECs, where $Co_3O_4$ monolayer microsphere arrays are directly grown on the rGO/CNTs film via a simple one-step hydrothermal deposition. This process avoids a troublesome two-step method (hydrothermal deposition and subsequent calcination) that is usually required to grow $Co_3O_4$ on some substrates (e.g., Cu foil, nickel foam, etc.), as reported previously.[21–23] Afterwards, electrochemical performance of the $Co_3O_4$/rGO/CNTs hybrid paper electrode for ECs is evaluated in a three-electrode system at room temperature. Interestingly, the as-prepared $Co_3O_4$/rGO/CNTs hybrid paper exhibits large SCs and good cycling stability at high rates in a 3 M KOH electrolyte, making such a hybrid paper a promising electrode for ECs applications.

## 2. Results and Discussion

### 2.1. Synthesis and Structural Analysis of the As-Prepared $Co_3O_4$/rGO/CNTs Hybrid Paper

**Figure 1** shows the X-ray diffraction (XRD) patterns of the GO/CNTs film and the $Co_3O_4$/rGO/CNTs hybrid paper. As observed in Figure 1a, the XRD pattern of the black GO/CNTs film (the inset) reveals an intense and sharp peak located at $2\theta$ = 10.8°, corresponding to the characteristic (001) diffraction of the GO. The interlayer spacing (0.81 nm) is much larger than that of natural graphite (ca. 0.34 nm), due to the introduction of oxygen-containing function groups on the graphite sheets and the CNTs between them.[24,25] Also, another visible peak at $2\theta$ = 26.5° can be attributed to the CNTs in the GO/CNTs film.[26,27] From the XRD pattern (Figure 1b) of the $Co_3O_4$/rGO/CNTs hybrid paper, seven pronounced diffraction peaks can be perfectly assigned to the (111), (220), (311), (400), (422), (440), and (533) planes of the cubic spinel $Co_3O_4$ (space group: FD-3m(227), JCPDS no. 43-1003). Interestingly, the sharp peak at $2\theta$ = 10.8° disappears and the peak at $2\theta$ = 26.5° can still be observed after hydrothermal deposition of $Co_3O_4$, as presented in Figure S1 (Supporting Information). Moreover, another peak $2\theta$ = 22.1° is also evident for the flexible hybrid paper (Figure S1, Supporting Information).[28,29] These XRD data indicate that the reduction of the GO has been successfully performed. Therefore, the alkaline hydrothermal treatment applied here not only facilities the formation of $Co_3O_4$ phase but also results in reduction of the GO, which can be further verified by the typical XRD pattern of rGO/CNT film, that is obtained by treating the pristine GO/CNTs film for the same alkaline hydrothermal process (Figure S2, Supporting Information). Although the underlying reduction mechanism remains unclear at this moment, the reduction of GO under alkaline conditions has also been reported by others.[30,31] Thus, the black $Co_3O_4$/rGO/CNTs flexible hybrid paper (the inset in **Figure 2**b) can be obtained after the facile one-step alkaline hydrothermal treatment.

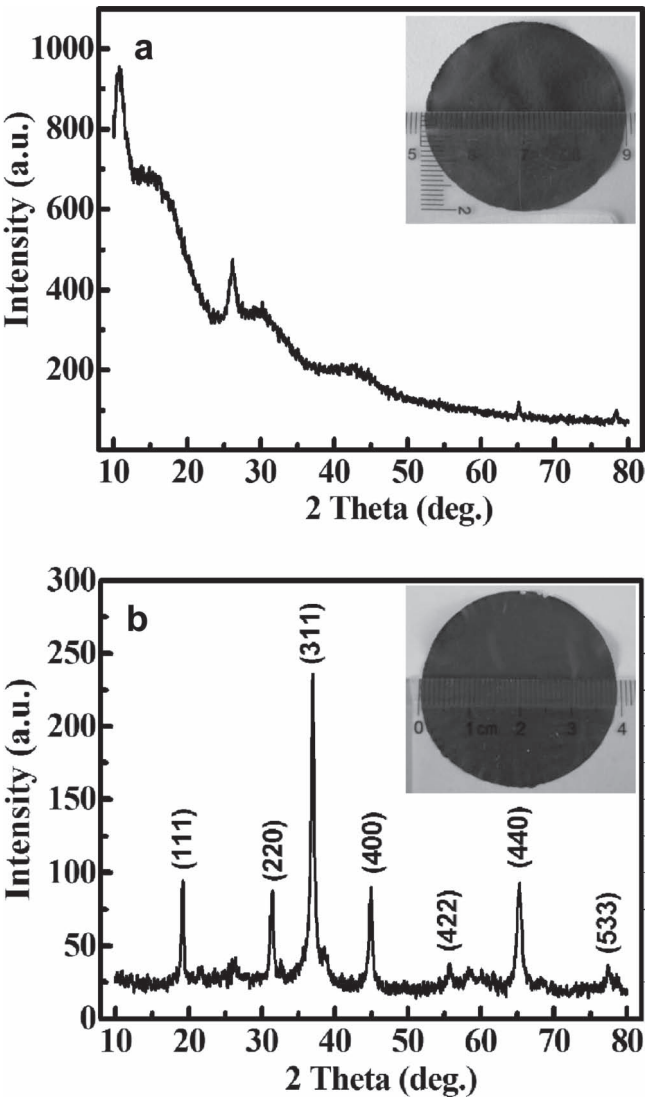


**Figure 1.** XRD patterns and optical images (insets) of a) the GO/CNTs film and b) the $Co_3O_4$/rGO/CNTs hybrid paper.

The more detailed composition of the $Co_3O_4$/rGO/CNTs hybrid paper is further characterized by X-ray photoelectron spectroscopy (XPS) and the corresponding results are presented in Figure 2. The Co 2p XPS spectrum (Figure 2a) shows two major peaks with binding energies at 779.85 and 794.82 eV, corresponding to Co $2p_{3/2}$ and Co $2p_{1/2}$, respectively, with a spin-energy separation of 14.97 eV, which is characteristic of a $Co_3O_4$ phase.[32–37] The high-resolution spectrum for the O 1s region (Figure 1b) shows two oxygen contributions from the $Co_3O_4$ and rGO. Particularly, the two core levels centered at 531.5 and 529.8 eV correspond to the oxygen species in the $Co_3O_4$ phase, the rGO and the –OH species absorbed onto the surface of these microspheres.[33,34,37] In addition, the C 1s

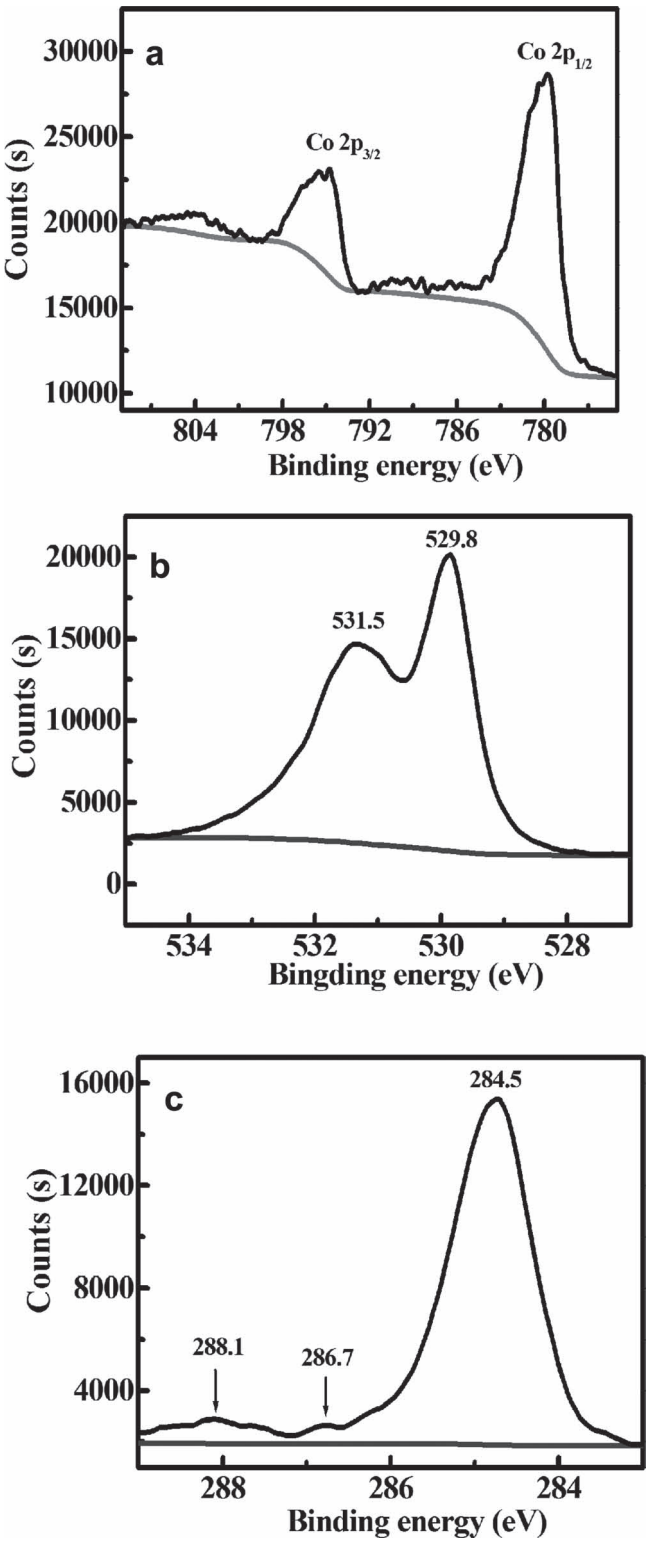


**Figure 2.** High-resolution XPS measurements for the Co 2p (a), O 1s (b), and C 1s (c) core levels for the $Co_3O_4$/rGO/CNTs hybrid paper.

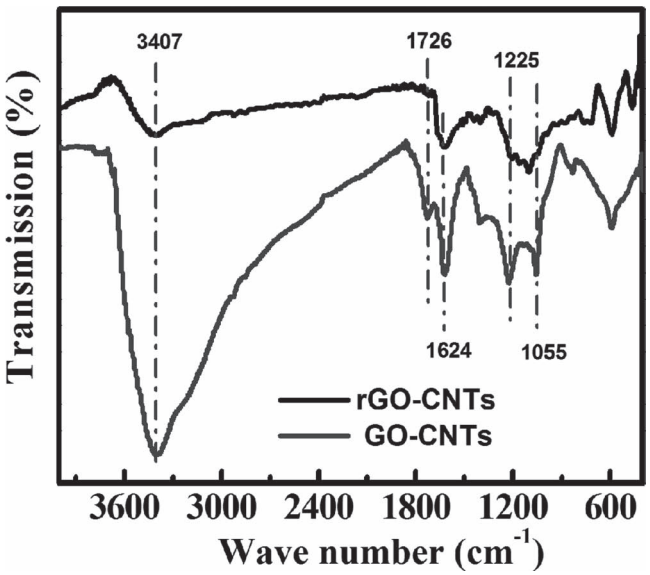


**Figure 3.** FTIR spectra of the GO/CNTs film and the rGO/CNTs film as indicated.

spectrum (**Figure 3**c) reveals the presence of three components of the carbon bond, i.e., C=O (286.7 eV), O=C=OH (288.1 eV), and C=C/C=C (284.5 eV), which are all in good agreement with the literature values.[36] It is interesting to note that the intensity of the peak associated with C=C/C=C becomes predominant, while the intensities of C=O and O=C=OH are dramatically reduced, compared to those reported in previous reports.[36–40] This indicates that most of the oxygen-containing functional groups have been successfully removed, which also can be confirmed by the Fourier transform infrared (FTIR) data.[36–40] As presented in Figure 3, the FTIR spectrum of the GO/CNTs film mainly exhibits five characteristic peaks. Specifically, the broad peak at 3407 $cm^{-1}$ is related to O–H stretching vibrations. The peaks at 1726, 1624, 1225, and 1055 $cm^{-1}$ can be assigned to C=O stretching motions of carboxylic acid and carbonyl moieties, C=C skeletal vibrations of unoxidized graphitic domains, C–OH stretching vibrations and C–O–C stretching vibrations, respectively. After alkaline treatment, the decreasing peaks in intensity at 3407 $cm^{-1}$ and the absence of the peaks at and 1726, 1225, and 1055 $cm^{-1}$ indicates that a great majority of functional groups have been removed. As a result, the electrical conductivity of the rGO/CNTs film is ca. 25.6 S $cm^{-1}$, which is ca. 50 times higher than that of the GO/CNTs film and favorable for the efficient energy storage. More importantly, the electrical conductivity of the $Co_3O_4$/rGO/CNTs hybrid paper can also remain as high as ca. 22 S $cm^{-1}$.

The heterostructure of the $Co_3O_4$/rGO/CNTs hybrid paper can be verified by morphological examination. Typical top-view field-emission scanning electron microscopy (FESEM) images over large area of the $Co_3O_4$/rGO/CNTs hybrid paper have been shown in **Figure 4**a,b. Apparently, $Co_3O_4$ microspheres with the size of ca. 1 μm are uniformly deposited on the surface of the rGO/CNTs film, in sharp contrast with the rGO/CNTs film (Figure S3a,b, Supporting Information). It is likely that the oxygen-containing functional groups (Figure 3), such as hydroxyl and carbonyl groups, on the surface of GO/CNTs film would act as anchor sites for the as-formed $Co_3O_4$ crystals. Figure 4c displays a cross-sectional FESEM image of the $Co_3O_4$/rGO/CNTs

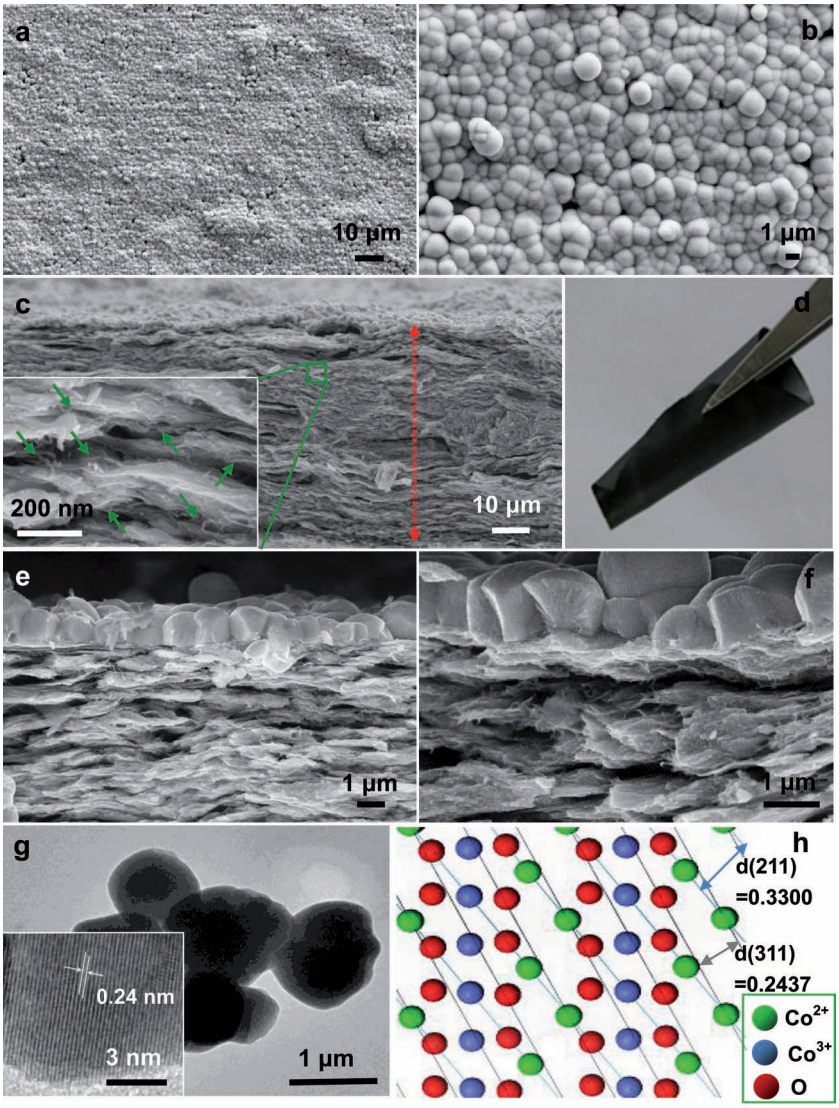


**Figure 4 a-h**

**Figure 4.** Typical a,b) top-view and c) side-view FESEM images of the flexible $Co_3O_4$/rGO/CNTs hybrid paper. The inset in (c) is the enlarged part of the region indicated by the green rectangle. The photograph in (d) demonstrates the flexibility of the paper. e,f) Enlarged cross-sectional view of the paper. g) TEM and HRTEM (the inset in g) images of $Co_3O_4$ microspheres. h) Atomic structure of the cubic phase $Co_3O_4$.

hybrid paper. It can be seen that the average thickness of the $Co_3O_4$/rGO/CNTs hybrid paper with a layered structure is ca. 50 μm. The $Co_3O_4$ microspheres are well-organized into a close-packed interconnected monolayer array, with a long range alignment that is both parallel and perpendicular to the rGO/CNTs films. The digital picture (Figure 4d) shows that the $Co_3O_4$/rGO/CNTs hybrid paper demonstrates good flexibility. In addition, the CNTs sandwiched between the rGO sheets as indicated by the green arrows (the inset in Figure 4c), can be evident. The unique layered structure results from the flow assembly effect during filtration. Closer examination (Figure 4d,e) reveals that the skeleton of the array grown on the layer-structured rGO/CNTs film is made of interconnected $Co_3O_4$ microsphere building blocks with a size of ca. 1 μm. To further clarify whether the $Co_3O_4$ phase also exists between the layers, energy dispersive analysis by X-ray (EDAX) line-scan element analysis of the cross-section of the flexible paper is performed. The line spectrum (Figure S4, Supporting Information) of the flexible hybrid paper shows the presence of Co element, suggesting that some $Co_3O_4$ can also exist between the layers of rGO/CNTs films, although large $Co_3O_4$ crystals cannot be found from the FESEM images, as shown in Figure 4e,f.

The $Co_3O_4$ content in the as-prepared hybrid paper can be facilely determined with TGA technique via oxidative decomposition. According to the mass loss of rGO/CNTs in the hybrid paper, as depicted in the thermogravimetric analysis (TGA) curve (Figure S5, Supporting Information), the weight fraction of $Co_3O_4$ in the hybrid paper is about 48 wt%. Figure 4g displays a transmission electron microscopy (TEM) image of the $Co_3O_4$ microspheres. Some solid microsphere-like particles with a size of ca. 1 μm can be clearly found, which is consistent with those in Figure 4e,f. The HRTEM image (the inset of Figure 4g) shows that an interplanar distance between adjacent lattice planes is 0.24 nm, which corresponds to the (311) plane of $Co_3O_4$ crystals (Figure 3h).

### 2.2. Formation Mechanism of the As-Prepared $Co_3O_4$/rGO/CNTs Hybrid Paper

Importantly, the construction of $Co_3O_4$/rGO/CNTs flexible film is performed by a facile one-step method, unlike those common two-step routes.[21–23] To investigate the major parameters that influence the one-step growth of $Co_3O_4$ phase on the surface of rGO/CNTs film, some other precipitants (such as, urea, L-lysine,[41,42] and KOH) and a different substrate (the rGO/CNTs film) are systematically studied.

As can be seen from Figure S6a (Supporting Information), except the peak ($2\theta = 26.5°$) ascribed the rGO/CNTs, other ten typical diffraction peaks of the as-synthesized hybrid paper by using urea as the precipitant can be successfully indexed to the cobalt carbonate hydroxide hydrate ($(Co(CO_3)_{0.5}(OH)_x \cdot 0.11H_2O$; JCPDS no. 48-0083), rather than the $Co_3O_4$ phase. Moreover, the pink sample grown on the rGO/CNTs presents uniform 3D nanowall-like arrays (Figure S6b–d, Supporting Information), and the nanowall is assembled by lots of cobalt carbonate hydroxide hydrate bundle with a diameter of ≈50–100 nm (Figure S6e,f, Supporting Information), which is wholly distinguished from that synthesized by using $NH_3 \cdot H_2O$ as the precipitant. In addition, when L-lysine and KOH are used as the precipitants, the samples grown on the rGO/CNTs are

both hexagonal phase $\beta$-$Co(OH)_2$ crystalline structure (Figure S7a and Figure S8a, Supporting Information), rather than $Co_3O_4$ and/or cobalt carbonate hydroxide hydrate. However, the $Co(OH)_2$ phase manifests as two wholly different morphologies. When L-lysine is used as the precipitant, the $Co(OH)_2$ exists as an aggregation of lots of small nanorods (Figure S7b–d, Supporting Information). On the other hand, flake-like $Co(OH)_2$ can be found (Figure S8b, Supporting Information) when KOH is used. As discussed above, therefore, it is evident to conclude that the precipitants greatly influence the compositions and morphologies of the hybrid papers, and the $NH_3 \cdot H_2O$ plays a significant role in the one-step growth of $Co_3O_4$ microspheres upon the rGO/CNTs film.

Furthermore, we directly use the rGO/CNTs as the substrate to deposit $Co_3O_4$ by using the precipitant of $NH_3 \cdot H_2O$. Figure S9a (Supporting Information) shows the XRD of as-synthesized sample using $NH_3 \cdot H_2O$ as precipitation and the rGO/CNTs film as deposition substrate. All the diffraction peaks can be indexed as the hexagonal phase $\beta$-$Co(OH)_2$ crystalline structure, which is consistent with the standard spectrum (JCPDS file no. 30-0443) with a space group of P-31(164). Interestingly, the pink sample grown upon the rGO/CNTs presents uniform 3D chrysanthemum-like structures with a diameter in the range of ≈6–8 μm, which are self-assembled in a radial way by numerous aligned cobalt hydroxide nanowires with the length of around 2 μm and a mean diameter of 100 nm (Figure S9b–f, Supporting Information). Unfortunately, once ultrasonication, the $Co(OH)_2$ chrysanthemum-like arrays have been wholly peeled off. Obviously, the weak adhesion to the underlying rGO/CNTs substrate presents. Here, the only difference is the use of rGO/CNTs as substrate rather than the GO/CNTs film. Clearly, the rGO owns much less oxygen content than the GO. Therefore, the higher amount of oxygen-containing species existing on the surface of GO may serve as oxidant to facilitate the formation of $Co_3O_4$ phase and enhance the adherence of $Co_3O_4$ to the rGO/CNTs substrate.

On the basis of our experimental results and the extensive discussion mentioned above, the synergetic effect of the precipitant $NH_3 \cdot H_2O$ and oxygen-containing functional groups on the GO surface on the formation of the unique hierarchical hybrid paper can be attentively put forward. Because of the unique hybrid structure, $Co_3O_4$ microsphere arrays firmly grown on the rGO/CNTs substrate with good electronic conductivity, this $Co_3O_4$/rGO/CNTs hybrid paper can directly serve as a working electrode for ECs.

### 2.3. Electrochemical Performance of the As-Prepared $Co_3O_4$/rGO/CNTs Hybrid Paper

Cyclic voltammetry (CV) and chronopotentiometry (CP) measurements are conducted in a three-electrode cell to evaluate the electrochemical properties of the $Co_3O_4$/rGO/CNTs hybrid paper. **Figure 5**a presents the representative CV curves of the hierarchical hybrid paper in 3 M KOH electrolyte at the scan rates of 5, 10, 20 mV $s^{-1}$. Well defined broad redox reaction peaks are visible in CV curves, indicating that the electrochemical capacitance of the $Co_3O_4$/rGO/CNTs flexible film is mainly contributed by the pseudocapacitance, as shown by Equation 1,2. Furthermore, the peak current increases with insignificant change in the CV shape when scan rates increase from 5 to 20 mV $s^{-1}$, which reveals its good electrochemical reversibility and high power characteristics.

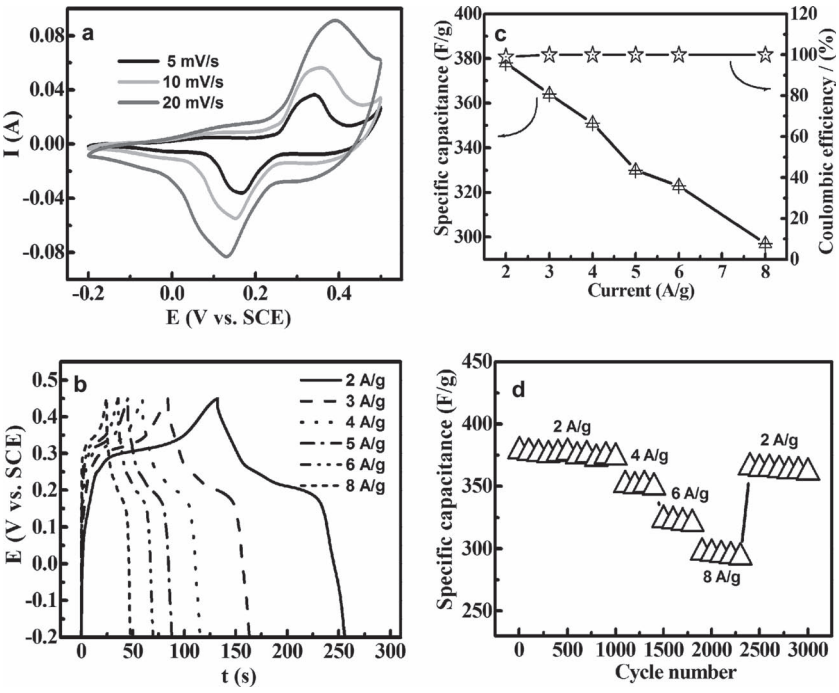


**Figure 5.** a) CV curves, b) CP plots, c) specific capacitance and coulombic efficiency as a function of current density, and d) cycling stability of the $Co_3O_4$/rGO/CNTs hybrid paper at progressive varying current densities.

$$Co_3O_4 + OH^- + H_2O \leftrightarrow 3CoOOH + e^- \quad (1)$$

$$CoOOH + OH^- \leftrightarrow CoO_2 + H_2O + e^- \quad (2)$$

On the contrary, the area under the current–potential curve and electrochemical response current density are extremely small even at 10 mV $s^{-1}$ for the rGO/CNTs film, suggesting that the SC of the rGO/CNTs film is very little, as shown in Figure S10a (Supporting Information).

To get more information about the potential of the as-synthesized $Co_3O_4$/rGO/CNTs hybrid paper as electrode materials for ECs, galvanostatic charge-discharge measurements are carried out in 3 M KOH solution between –0.2 to 0.45 V (vs. SCE) at different current densities ranging from 2 to 8 A $g^{-1}$, as shown in Figure 5b. The observed mirror-like potential-time response implies the high charge-discharge columbic efficiency (not less than 99.5%) of the paper electrode at all the current densities, as shown in Figure 5c. The SCs of the flexible paper electrode can be calculated based on the charge-discharge curves in Figure 4b and the typical data are plotted

in Figure 4c. Evidently, the flexible paper electrode exhibits excellent pseudocapacitances of 378, 364, 351, 330, 323, and 297 F $g^{-1}$ at 2, 3, 4, 5, 6, and 8 A $g^{-1}$, respectively. This also suggests that 78% of the capacitance is still retained when the charge–discharge rate changes from 2 to 8 A $g^{-1}$, which is even better than other $Co_3O_4$/rGO electrodes.[43–45] And based on the CP data (Figure S10b, Supporting Information), the SCs of 5.8, 5.3, 5, 4.7, 4.4, and 4 F $g^{-1}$ are delivered by the rGO/CNTs film at 2, 3, 4, 5, 6, and 8 A $g^{-1}$, respectively, which clearly proves that the main contribution of the measured SCs of the $Co_3O_4$/rGO/CNTs film is from the pseudocapacitive surface redox process of $Co_3O_4$ species grown on the rGO/CNTs film, rather than the rGO/CNTs film itself. Considering the loading of $Co_3O_4$, a SC contribution of ca. 781 F $g^{-1}$ can be obtained at a current density of 2 A $g^{-1}$ by the $Co_3O_4$ phase in the hybrid paper. The cycling performance of the flexible paper at progressively increased current densities is recorded as shown in Figure 5d. Obviously, the flexible paper electrode exhibits stable cycling performance at each current density. After 2300 times of continuous cycling at varying current densities, the current density is returned to 2 A $g^{-1}$. Under this condition, ca. 96% of the initial capacitance at 2 A $g^{-1}$ can still be recovered and maintained for another 700 cycles without noticeable decrease. The data in Figure 4d highlights the capability of the flexible paper electrode to meet the requirements of both long cycle life and good rate capability, which are important merits for the practical energy storage devices.

The large SCs and good cycling stability of our $Co_3O_4$/rGO/CNTs flexible hybrid paper are attributed to the intimate integration between the rGO/CNTs film with good electronic conductivity and the $Co_3O_4$ microsphere array grown directly on it. Specifically, charges could be effectively and rapidly conducted back and forth from the electroactive $Co_3O_4$ microsphere array and the rGO/CNTs collector through the highly conducting three-dimensional network. The rGO/CNTs support can also ensure good dispersion of the $Co_3O_4$ microsphere array, a desirable feature for enhancing the cycling stability.

## 3. Conclusions

In summary, we have developed a facile one-step method to synthesize flexible and free-standing $Co_3O_4$/rGO/CNTs paper electrodes for electrochemical capacitors. In this unique hybrid paper, a monolayer $Co_3O_4$ microsphere array is grown directly on the rGO/CNTs film over large area. Comparative experiments confirm that the precipitant of $NH_3 \cdot H_2O$ and oxygen-containing functional groups on GO surface synergistically contribute to the one-step formation of the $Co_3O_4$ phase on the rGO/CNTs film. Electrochemical evaluation reveals that this unique flexible paper electrode can deliver an SC of 378 F $g^{-1}$ at 2 A $g^{-1}$ and 297 F $g^{-1}$ at 8 A $g^{-1}$ with excellent electrochemical stability. The desirable electrochemical performance of the flexible paper electrode stems mainly from the unique hierarchical microstructure. The present structural design approach offers an effective and convenient technique to boost the specific capacities, rate capability, and cycling stability of electrode materials for ECs, which is particularly useful for lithium-ion battery applications.

## 4. Experimental Section

*Synthesis of $Co_3O_4$/rGO/CNTs Flexible Paper*: All the chemicals were of analytical grade and were used without further purification. GO was synthesized from natural graphite by a modified Hummers method as described elsewhere.[36,38] As-synthesized GO was suspended in water to give a brown dispersion, which was then subjected to dialysis to completely remove residual salts and acids. CNTs were purchased from Nanotech Port Co. (Shenzhen China) and purified by refluxing in nitric acid ($HNO_3$) at 40 °C for 4 h before use. The GO/CNTs hybrid film was prepared by the following process. GO (27.5 mg) was dispersed in distilled water (50 mL) by ultrasonication for 1 h. After adding 5.5 mg of CNTs, the mixture was sonicated for another 30 min and then filtered by a vacuum filter equipped with a 0.2 μm porous polytetrafluoroethylene (PTFE) membrane to obtain a GO/CNTs hybrid film. $Co(NO_3)_2 \cdot 6H_2O$ (10 mmol) and $NH_4NO_3$ (5 mmol) were dissolved in a solution consisting of 35 mL of $H_2O$ and 18 mL of ammonia (25 wt%). Then, the homogeneous solution and the GO/CNTs film were then transferred into a Teflon-lined stainless steel autoclave. The autoclave was sealed and maintained at 90 °C for 14 h. After cooled to room temperature, the flexible hybrid paper was rinsed under ultrasonication, and dried at 80 °C for 12 h. For comparison, some samples were also made by using other precipitants (urea ($CO(NH_2)_2$), L-lysine, and KOH) while other synthesis conditions were kept the same. Additionally, the rGO/CNTs film was prepared by treating the GO/CNTs film in the same hydrothermal process but without adding $Co(NO_3)_2 \cdot 6H_2O$.

*Materials Characterization*: The samples were examined by powder XRD (Max 18 XCE, Japan) using a Cu $K_a$ source ($\lambda$ = 0.1542 nm) at a scanning speed of 3° $min^{-1}$ over a 2$\theta$ range of 10–80°. The morphology was observed with field-emission scanning electron microscopy (FESEM; JEOL-6300F, 15 kV) and TEM (FEI, TECNAI-20). XPS measurements were performed on a VGESCALAB MKII X-ray photoelectron spectrometer with a $Mg_{ka}$ excitation source (1253.6 eV). FTIR spectra were recorded with a Model 360 Nicolet AVATAR. TGA measurements were carried out under nitrogen flow with a NETZSCH STA 409 PC system TG Analyzer at a heating rate of 10 °C $min^{-1}$. Electrical conductivity was measured by the conventional four-probe DC method (SDY-5 Four-Point probe meter).

*Electrochemical Tests*: The $Co_3O_4$/rGO/CNTs flexible paper acted directly as the working electrode for the following electrochemical tests by CV and CP, performed with a CHI660C electrochemical workstation. All measurements were carried out in a three compartment cell with a working electrode, a platinum plate counter electrode, and a saturated calomel electrode (SCE) as the reference electrode at room temperature. The electrolyte was a 3 M KOH aqueous solution.

The SCs of the $Co_3O_4$/rGO/CNTs flexible paper electrode or the rGO/CNTs electrode were calculated from the CP curves based on the following equation:

$$C = \frac{It}{\Delta V} \tag{3}$$

where $C$, $I$, $t$, and $\Delta V$ are the SC (F $g^{-1}$) of the electrodes, the discharging current density (A $g^{-1}$), the discharging time (s), and the discharging potential range (V), respectively. Also, the SCs of $Co_3O_4$ was obtained according to the following equation:[26,46]

$$C_{Co_3O_4} = \frac{C_{Co_3O_4/rGO/CNTs} - (1 - w_{Co_3O_4})C_{rGO/CNTs}}{w_{Co_3O_4}} \tag{4}$$

where $C_{Co_3O_4/rGO/CNTs}$, $C_{Co_3O_4}$, $w_{Co_3O_4}$, $C_{rGO/CNTs}$ are the SC of $Co_3O_4$ in the $Co_3O_4$/rGO/CNTs flexible paper, the percentage of $Co_3O_4$ in the flexible paper and the SC of the rGO/CNTs film, respectively.

An important parameter, the columbic efficiency ($\eta$) of the electrode, was evaluated from the following equation based on the CP plots depicted in Figure 3c:

$$\eta = \frac{t_D}{t_C} \times 100\% \tag{5}$$

where $t_D$ and $t_C$ are the time for galvanostatic discharging and charging, respectively.

## Supporting Information

Supporting Information is available from the Wiley Online Library or from the author.

## Acknowledgements

The authors gratefully acknowledge the financial support of the National Natural Science Foundation of PRC (no. 20873064, 21173120), Natural Science Foundation of Anhui Province (no. 10040606Q07), Natural Science Foundation of Jiangsu Province (no. BK2011030), Specialized Research Fund for the Doctoral Program of Higher Education of China (no. 20060287026), 2010 Young Teachers' Foundation of Anhui University of Technology (no. QZ201003), and Graduate Innovation Program of Anhui University of Technology (2011009).

Received: November 25, 2011
Revised: December 27, 2011
Published online: March 30, 2012

[1] B. E. Conway, *Electrochemical Supercapacitors: Scientific Fundamentals and Technological Applications*, Kluwer, New York **1999**.
[2] R. F. Service, *Science* **2006**, *313*, 902.
[3] P. Simon, Y. Gogotsi, *Nat. Mater.* **2008**, *7*, 845.
[4] C. Z. Yuan, B. Gao, L. F. Shen, S. D. Yang, L. Hao, X. J. Lu, F. Zhang, L. J. Zhang, X. G. Zhang, *Nanoscale* **2011**, *3*, 529.
[5] X. H. Xia, J. P. Tu, X. L. Wang, C. D. Gu, X. B. Zhao, *Chem. Commun.* **2011**, *47*, 5786.
[6] L. R. Hou, C. Z. Yuan, L. Yang, L. F. Shen, F. Zhang, X. G. Zhang, *RSC Adv.* **2011**, *1*, 1521.
[7] Y. Y. Liang, M. G. Schwab, L. J. Zhi, K. U. Mugnaioli, X. L. Feng, K. Müllen, *J. Am. Chem. Soc.* **2010**, *132*, 15030.
[8] H. T. Wang, L. Zhang, X. H. Tan, C. M. B Holt, B. Zahiri, B. C. Olsen, D. Mitlin, *J. Phys. Chem. C* **2011**, *115*, 17599.
[9] D. W. Wang, Q. H. Wang, T. M. Wang, *Inorg. Mater.* **2011**, *50*, 6482.
[10] W. Xiao, J. S. Chen, X. W. Lou, *J. Mater. Chem.* **2010**, *20*, 7015.
[11] M. B. Zheng, J. Cao, S. T. Liao, J. S. Liu, H. Q. Chen, Y. Zhao, W. J. Dai, G. B. Ji, J. M. Cao, J. Tao, *J. Phys. Chem. C* **2009**, *113*, 3887.
[12] C. Z. Yuan, X. G. Zhang, L. H. Su, B. Gao, L. F. Shen, *J. Mater. Chem.* **2009**, *19*, 5772.
[13] Y. G. Wang, H. Q. Li, Y. Y. Xia, *Adv. Mater.* **2006**, *18*, 2619.
[14] H. L. Wang, H. S. Casalongue, Y. Y. Liang, H. J. Dai, *J. Am. Chem. Soc.* **2011**, *132*, 7472.
[15] E. Yoo, J. Kim, E. Hosono, H. S. Zhou, T. Kudo, I. Honma, *Nano Lett.* **2008**, *8*, 2277.
[16] X. J. Lu, H. Dou, B. Gao, C. Z. Yuan, S. D. Yang, L. Hao, L. F. Shen, X. G. Zhang, *Electrochim. Acta* **2011**, *56*, 5115.
[17] Z. J. Fan, J. Yan, L.J. Zhi, Q. Zhang, T. Wei, J. Feng, M. L. Zhang, W. Z. Qian, F. Wei, *Adv. Mater.* **2010**, *22*, 3723.
[18] D. S. Yu, L. M. Dai, *J. Phys. Chem. Lett.* **2010**, *1*, 467.
[19] V. C. Tung, L. M. Chen, M. J. Allen, J. K. Wassei, K. Nelson, R. B. Kaner, Y. Yang, *Nano Lett.* **2009**, *9*, 1949.
[20] H. Gwon, H. S. Kim, K. U. Lee, D. H. Seo, Y. C. Park, Y. S. Lee, B. T. Ahn, K. Kang, *Energy Environ. Sci.* **2011**, *4*, 1277.
[21] G. L. Wang, D. X. Cao, C. L. Yin, Y. Y. Gao, J. L. Yin, L. Chen, *Chem. Mater.* **2009**, *21*, 5112.
[22] X. Y. Xue, S. Yuan, L. L. Xing, Z. H. Chen, B. He, Y. J. Chen, *Chem. Commun.* **2011**, *47*, 4718.
[23] Y. Y. Gao, S. L. Chen, D. X. Cao, G. L. Wang, J. L. Yin, *J. Power Sources* **2010**, *195*, 1757.
[24] C. Xu, X. Wu, J. Zhu, X. Wang, *Carbon* **2007**, *46*, 386.
[25] S. Chen, J. W. Zhu, X. D. Wu, Q. F. Han, X. Wang, *ACS Nano* **2010**, *4*, 2822.
[26] C. Z. Yuan, L. Chen, B. Gao, L. H. Su, X. G. Zhang, *J. Mater. Chem.* **2009**, *19*, 246.
[27] C. Z. Yuan, S. L. Xiong, X. G. Zhang, L. F. Shen, Fang Zhang, B. Gao, L. H. Su, *Nano Res.* **2009**, *2*, 722.
[28] Z. P. Li, J. Q. Wang, S. Liu, X. H. Liu, S. R. Yang, *J. Power Sources* **2011**, *196*, 8160.
[29] L. H. Tang, Y. Wang, Y. M. Li, H. B. Feng, J. Lu, J. H. Li, *Adv. Funct. Mater.* **2009**, *19*, 2782.
[30] R. R. Wang, J. Sun, L. Gao, C. H. Xu, J. Zhang, Y. Q. Liu, *Nanoscale* **2011**, *3*, 904.
[31] X. B. Fan, W. C. Peng, Y. Li, X. Y. Li, S. L. Wang, G. L. Zhang, F. B. Zhang, *Adv. Mater.* **2008**, *20*, 4490.
[32] C. D. Wanger, D. J. F. Rigga, M. G. E. Moulder, *Handbook of X-ray Photoelectron Spectroscopy*, Perkin-Elmer, Eden Prairie **1978**.
[33] S. L. Xiong, C. Z. Yuan, X. G. Zhang, B. J. Xi, Y. T. Qian, *Chem. Eur. J.* **2009**, *15*, 5320.
[34] S. C. Petitto, M. A. Langell, *J. Vac. Sci. Technol.* **2004**, *A22*, 1690.
[35] J. Yang, H. W. Liu, W. N. Martens, R. L. Frost, *J. Phys. Chem. C*, **2010**, *114*, 111.
[36] J. Yan, T. Wei, W. M. Qiao, B. Shao, Q. K. Zhao, L. J. Zhang, Z. J. Fan, *Electrochim. Acta* **2010**, *55*, 6973.
[37] C. Z. Yuan, L. Yang, L. R. Hou, L. F. Shen, F. Zhang, D. K. Li, X. G. Zhang, *J. Mater. Chem.* **2011**, *21*, 18183.
[38] S. Stankovich, D. A. Dikin, R. D. Piner, K. A. Kohlhaas, A. Kleinhammes, Y. Y. Jia, Y. Wu, S. T. Nguyen, R. S. Ruoff, *Carbon* **2007**, *45*, 1558.
[39] J. B. Liu, S. H. Fu, B. Yuan, Y. L. Li, Z. X. Deng, *J. Am. Chem. Soc.* **2010**, *132*, 7279.
[40] H. K. Jeong, Y. P. Lee, R. J. W. E. Lahaye, M. H. Park, K. H. An, L. J. Kim, C. W. Yang, C. Y. Park, R. S. Ruoff, Y. H. Lee, *J. Am. Chem. Soc.* **2008**, *130*, 1362.
[41] C. Z. Yuan, X. G. Zhang, L. R. Hou, L. F. Shen, D. K. Li, F. Zhang, C. G. Fan, J. M. Li, *J. Mater. Chem.* **2010**, *20*, 10809.
[42] C. Z. Yuan, L. Yang, L. R. Hou, D. K. Li, L. F. Shen, F. Zhang, X. G. Zhang, *J. Solid State Electrochem.* **2011**, DOI:10.1007/s1008-011-1549-7.
[43] J. Yan, T. Wei, W. M. Qiao, B. Shao, Q. K. Zhao, L. J. Zhang, Z. J. Fan, *Electrochim. Acta* **2010**, *55*, 6973.
[44] W. W. Zhou, J. P. Liu, T. Chen, K. S. Tan, X. T. Jia, Z. Q. Luo, C. X. Cong, H. P. Yang, C. M. Li, T. Yu, *Phys. Chem. Chem. Phys.* **2011**, *13*, 14462.
[45] H. W. Wang, Z. A. Hu, Y. Q. Chang, Y. L. Chen, Z. Y. Zhang, Y. Y. Yang, H. Y. Wu, *Mater. Chem. Phys.* **2011**, *130*, 672.
[46] C. C. Hu, W. C. Chen, *Electrochim. Acta* **2004**, *49*, 3469.